Raman Microspectroscopic Study of the Cation Distribution in Amphiboles

A. WANG, P. DHAMELINCOURT, and G. TURRELL*

Laboratory of Physical Mineralogy, Chinese Academy of Geological Sciences, Beijing, China (A.W.); and Laboratoire de Spectrochimie Infrarouge et Raman, CNRS, Université des Sciences et Techniques de Lille Flandres Artois, Bât. C.5, 59655 Villeneuve d'Ascq Cedex, France (P.D., G.T.)

The first attempt to determine the cation distributions in amphiboles by Raman microspectroscopy is described. The Raman spectra of five amphibole samples were obtained. It was observed that the Raman bands of the OH stretching modes were narrower than the corresponding infrared bands previously reported. However, even with the use of the most sophisticated Raman instruments, it was not possible to distinguish the bands due to the different cation arrangements of one particular configuration. Nevertheless, the experimental results and the theoretical analysis developed here allowed approximate calculations of the site occupancies to be made for four samples. These results yield a better understanding of the problems involved in the determination of the cation distributions in amphiboles with the use of vibrational spectroscopic methods.

Index Headings: **Raman microspectroscopy; Amphiboles; Cation distribution.**

INTRODUCTION

The distribution of cations in the amphiboles is a problem of particular interest to mineralogists. However, on the basis of the results of elemental analysis, the site occupancy can only be inferred from the theoretical structural formula for the amphibole and the application of certain empirical rules for the distribution of the cations among the various crystallographic sites. The true cation distributions in these minerals have not been susceptible to direct measurement.

In the past twenty years, spectroscopic methods have entered the mineralogical field and have developed very rapidly in certain applications. It is now possible to measure, at least partially, the true site occupancy in amphiboles having simple compositions, with the use of Mössbauer, infrared, and electron absorption spectroscopies. The combined results of the application of these techniques and elemental analysis allow the problem of cation distribution in some of the amphiboles to be resolved.

The early application of Mössbauer spectroscopy in this area was made by Bancroft *et al.*,[1,2] and this subject is still attracting the interest of many Mössbauer spectroscopists.[3] Through the analysis of quadrupole splitting, this method can distinguish quantitatively between the $M(4)$ and $M(1)$, $M(2)$, and $M(3)$ site occupancy by the Fe^{2+} and Fe^{3+} cations in most amphiboles. However, because of the crystallographic similarity of the $M(1)$, $M(2)$, and $M(3)$ sites, the corresponding doublets cannot be resolved. Thus, it is difficult to obtain useful information on the occupancy of these sites with the Mössbauer technique.

On the other hand, the study by infrared spectroscopy of the OH stretching vibrations of many amphiboles offers very interesting complementary information on the $M(1)$ and $M(3)$ site occupancies. In particular, Burns and co-workers,[4-6] Strens,[7,8] and Law[3,9] have reported very valuable results in this domain. In the amphibole lattice, the OH groups lie on $O(3)$ sites; their nearest neighbors are one $M(3)$ site and two $M(1)$ sites. Thus, the OH groups interact strongly with the cations which occupy these sites. An analysis of the structure of the amphiboles shows that the interaction force field, which has pseudotrigonal symmetry, will change with the cation occupancy of the $M(1)$ and $M(3)$ sites. Therefore, the OH vibrational frequencies provide a direct indication of cation occupancy, and, by decomposition of the complex structure of the observed OH bands, it is possible to deduce the $M(1)$ and $M(3)$ site occupancies by the different cations.

Very few Raman spectroscopic investigations of amphiboles have been reported,[10,11] and, apparently, no attempts have been made to use the Raman spectra of the OH stretching modes to determine the cation distribution. It should be noted, however, that many amphibole samples exhibit strong fluorescence, which generally masks the Raman spectrum; thus, it is very difficult to obtain good Raman spectra with traditional spectrometers. However, Raman microspectroscopic methods allow a very small area ($\sim 1\ \mu m^2$) near the surface of the sample to be chosen. It is often possible to select an area in which fluorescence is minimal.[12] Moreover, the use of signal averaging techniques results in a significant increase in the signal-to-noise ratio. Thus, the spectrum of the OH stretching vibrations, as well as the low-frequency region, can be recorded for many members of the series of amphiboles.

In the present work, five different amphiboles have been investigated by Raman microspectroscopy. An attempt has been made in each case to determine the site occupancy by treating the recorded multicomponent spectra with a decomposition program. Comparison of the results of the spectral decomposition with the predicted number of vibrational modes has allowed an approximate calculation to be made of both the site occupancies and the segregation parameters in binary systems.

THEORETICAL ANALYSIS

The formula for the amphiboles can be written

$$A_{0-1}B_2C_5T_8O_{22}(OH,F,Cl)_2. \quad (1)$$

Like all double-chain silicates, these structures consist of pairs of chains parallel to the crystallographic c axis.

Received 11 January 1988; revision received 27 May 1988.

* Author to whom correspondence should be sent.

0003-7028/88/4208-1441$2.00/0

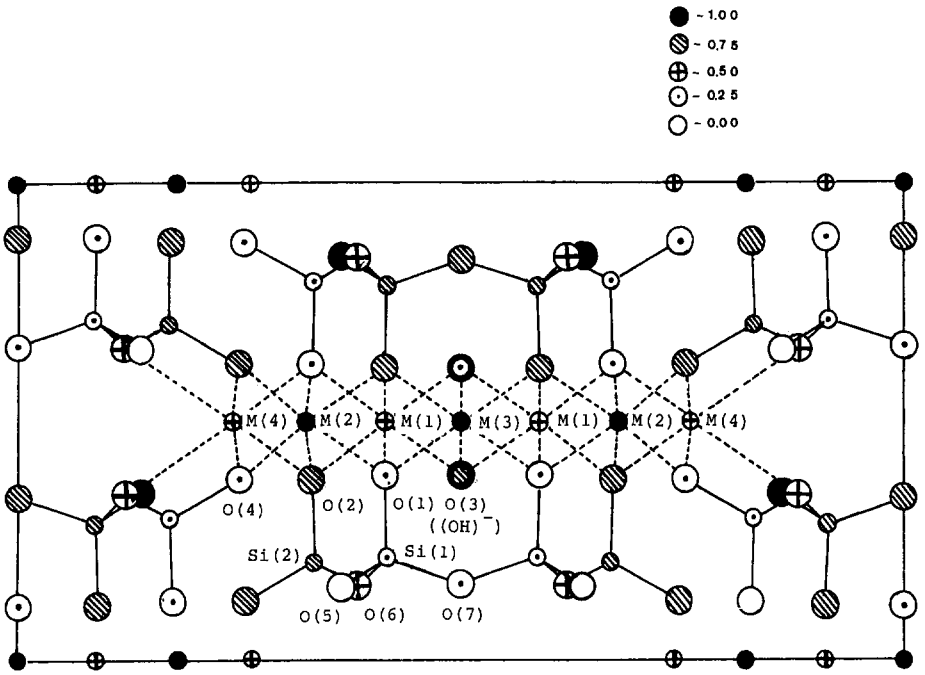

FIG. 1. Crystal structure of amphiboles.

Each chain is composed of SiO_4 tetrahedra connected by their vertices. The nonbridging oxygens (NBO) of these chains form polyhedral spaces for the cations, as shown in Fig. 1. The $M(1)$, $M(2)$, and $M(3)$ sites are nearly regular octahedrons with a coordination number equal to six; they are often occupied by C cations such as Mg^{2+}, Fe^{2+}, Fe^{3+}, Al^{3+}, and Mn^{2+}, Ti^{4+}, . . . , etc. Generally, the bivalent cations are found to occupy $M(1)$ and/or $M(3)$ sites, while the smaller Fe^{3+}, Al^{3+}, and Ti^{4+} ions are in $M(2)$ sites. The $M(4)$ sites are distorted dodecahedra with a coordination number equal to eight. They are often occupied by the larger B cations such as Ca^{2+}, although Fe^{2+}, Mg^{2+}, Na^+, K^+, . . . , etc., can also enter these sites. The largest sites (A) are always occupied by the largest cations, such as K^+, Na^+, . . . , etc. When there are not enough A cations in the lattice, some of these sites remain empty.

Factor-group Analysis. The amphiboles are of two structural types, although most of them belong to the monoclinic system and are of space group $C2/m$. The site symmetries of the ions according to the results of x-ray structural refinement are given in Table I. By assuming that the hydrogen atoms also have C_s site symmetry, factor-group analysis yields the number and activity of the vibrational modes for this type of amphibole, *viz.*,

$$\Gamma_{vib} = 30\,A_g(R) + 30\,B_g(R) + 28\,A_u(IR) + 35\,B_u(IR). \quad (2)$$

For the infrared-active modes, one A_u and two B_u modes arise from the contribution of A cations. If the A sites are empty (as for Cummingtonite), the number of infrared-active modes will be reduced to 27 A_u and 33 B_u.

In order to classify these modes by means of the correlation method, it has been assumed that the polyatomic OH^- and $Si_4O_{11}^{4-}$ ions have C_s symmetry in the lattice. The complete results are given in Table II. Among the 123 vibrational modes there are 43 lattice modes for which the Raman (A_g, B_g)- and infrared (A_u, B_u)-active modes correspond to the in-phase and out-of-phase translational and librational movements, respectively, of the two anion groups and the two cations. The direction of the movements, e.g., the axis along which the ions translate or the axis around which they rotate, are denoted in Table II by subscripts which refer to the corresponding number of the lattice mode.

The vibrations corresponding to the internal modes are more difficult to describe. The isolated $Si_4O_{11}^{4-}$ ions have C_s symmetry, as shown in Fig. 2; thus, according to group theory there are 39 vibrational modes and

$$\Gamma_{vib}(Si_4O_{11}^{4-}) = 20A'(IR,R) + 19A''(IR,R). \quad (3)$$

In the primitive cell of monoclinic amphiboles there are two $Si_4O_{11}^{4-}$ groups, whose site symmetry is also C_s. With the use of the correlation method the number of vibrational modes due to the $Si_4O_{11}^{4-}$ ions can be determined (see Table III). Thus,

$$\Gamma_{inter.}(Si_4O_{11}^{4-}) = 20A_g(R) + 19B_g(R) + 19A_u(IR) + 20B_u(IR). \quad (4)$$

For the isolated OH^- ions, the only vibrational mode is the stretch, Σ^+ (point group $C_{\infty v}$). In the primitive cell of monoclinic amphiboles there are two OH^- ions, which are surrounded by the cations located in $M(1)$ and $M(3)$

TABLE I. Site symmetry in monoclinic amphiboles.

Ions	Number	Wyckoff notation	Site symmetry
$M(1)$, $M(4)$	2	4*h*	C_2
$M(2)$	2	4*g*	C_2
$M(3)$	1	2*a*	C_{2h}
A	1	2*b*	C_{2h}
Si(1), *Si*(2)	4	8*j*	C_1
$O(1)$, $O(2)$, $O(4)$, $O(5)$, $O(6)$	2	8*j*	C_1
$O(3)(OH^-)$, $O(7)$	2	4*i*	C_s

TABLE II. Classification of vibrational modes.

	Γ_{trans}					Γ^{OH^-}			$\Gamma^{Si_4O_{11}^{4-}}$				
	A	$M(3)$	$M(1)$	$M(2)$	$M(4)$	Trans	Rot	Vib	Trans	Rot	Vib	Γ_{acoust}	Γ_{vib}
A_g(R)			1_z	1_z	1_z	$2_{x,y}$	1_c	1	$2_{x,y}$	1_z	20		30
B_g(R)			$2_{x,y}$	$2_{x,y}$	$2_{x,y}$	1_z	1_b		1_z	$2_{x,y}$	19		30
A_u(IR)	1_z	1_z	1_z	1_z	1_z	1_z	1_c		1_z	$2_{x,y}$	19	1	28
B_u(IR)	$2_{x,y}$	$2_{x,y}$	$2_{x,y}$	$2_{x,y}$	$2_{x,y}$	$2_{x,y}$	1_b	1	$2_{x,y}$	1_z	20	2	25
Total	3	3	6	6	6	6	4	2	6	6	78	3	123

sites. Thus there will be two internal vibrational modes for these ions (See Table IV), and

$$\Gamma_{inter.}(OH^-) = A_g(R) + B_u(IR). \quad (5)$$

According to the classification of these modes in the C_{2h} point group, the A_g species will correspond to the in-phase stretching motion of two OH^- ions within the unit cell, while the B_u species represents the corresponding out-of-phase movement. Consequently, the same number of OH stretching bands will be observed in the Raman and infrared spectra of amphiboles, although the symmetries of these vibrations are different.

Site-occupancy Formulas. Figure 3, which shows the local environment of the two OH^- ions in the Cummingtonite lattice, was drawn in accordance with the crystal structure refinement results.[13] By simple geometrical calculation it can be shown that the distances between the oxygen atoms and the $M(1)$ and $M(3)$ positions are almost equal; thus,

$$L_{O(3)M(1)} = L_{O(3)M'(1)} = L_{O'(3)M(1)} = L_{O'(3)M'(1)} = 2.098_1 \text{ Å} \quad (6)$$

and

$$L_{O(3)M'(3)} = L_{O'(3)M(3)} = 2.074_4 \text{ Å}. \quad (7)$$

On the other hand, according to the results of the work of Burns and Strens,[4] the OH bond is almost perpendicular to the crystallographic axis c, and the angle is equal to 85 ± 8°. If the length of the OH bond is taken to be 1 Å, as found in many crystallographic references,[14] the distances between the hydrogen atoms and the $M(1)$ and $M(3)$ positions can be calculated. These distances are also nearly equal, with:

$$L_{HM(1)} = L_{HM'(1)} = L_{H'M(1)} = L_{H'M'(1)} = 2.7408 \text{ Å} \quad (8)$$

and

$$L_{HM'(3)} = L_{H'M(3)} = 2.7228 \text{ Å}. \quad (9)$$

Each OH^- ion is then located on the approximately ternary axis of a slightly distorted trigonal system. For the OH^- ion, $M(1)$ and $M'(1)$ are still equivalent sites, but the $M(3)$ site is not. For different distributions of the cations in these three sites, different noncentrosymmetric interaction forces will influence the movement of the OH^- ion. The obvious result of this interaction is that several OH stretching vibrational bands will appear in the 3600–3700 cm^{-1} region. The multicomponent pattern similar to that observed in the infrared spectra would also be expected in the Raman spectra.

It was mentioned before that the C cations Mg^{2+}, Fe^{2+}, Fe^{3+}, Al^{3+}, . . . , etc., have the possibility of entering the $M(1)$ and $M(3)$ sites. Therefore, according to the nature of the cations, and considering all the possibilities of distributing these cations among the different sites, it is possible to deduce theoretically the number of OH stretching bands which should be observed. For example, four configurations exist for the binary system and eight OH bands are expected to be observed. Similarly, 20 OH bands are predicted for the ternary system, and 42 for the quaternary system. The site occupancy and the related number of OH bonds are given in Table V.

If it were possible to observe all these bands, the $M(1)$ and $M(3)$ site occupancy for each cation could be calculated, assuming that the transition moment of the OH stretch is independent of the different configurations. The last row of Table V is used to obtain the formula for the site occupancy, in which the numbers represent the coefficient of each term in the formula. For example, the $M(3)$ site occupancy of Mg^{2+} for the ternary system is given by:

$$Mg^{2+}(M(3)) = \mu_3 = (A + 2B'' + C' + 2E'' + G' + 2F)/W \quad (10)$$

where W is the sum of all of the OH stretching band intensities. Unfortunately, in infrared and Raman spectroscopy the spectral resolution of the instruments has not attained a level where B' and B'' bands, and C' and C'' bands, etc., can be resolved. Under these conditions only the total occupancy of the $M(1)$ and $M(3)$ sites for each cation can be determined. For example, the $M(1)$

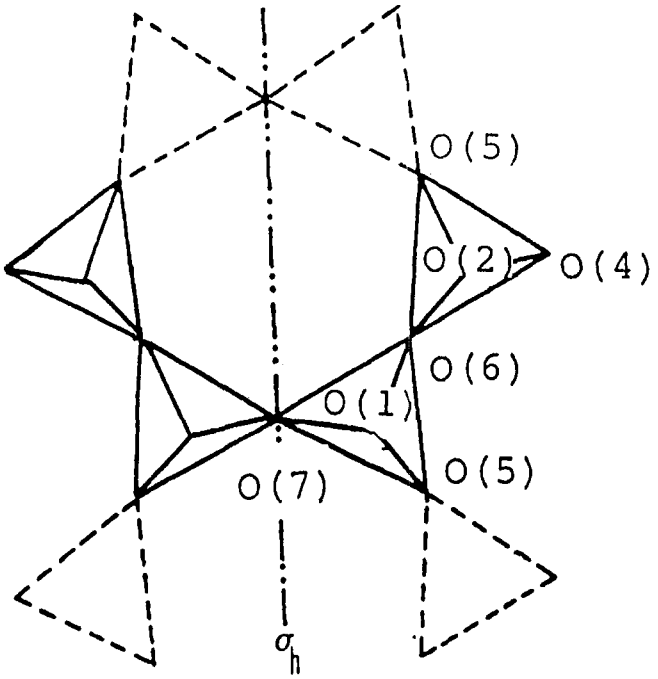

FIG. 2. Symmetry of the $Si_4O_{11}^{4-}$ ion.

TABLE III. Internal vibrational modes of the $Si_4O_{11}^{4-}$ groups.

Molecular sym.		Site sym.		Factor group sym.	
C_s	$N = 2$ →	C_s	→	C_{2h}	
t^v	f^v				a^v
20	A' — 40 —	A'		A_g	20
				B_g	19
19	A'' — 38 —	A'		A_u	19
				B_u	20

TABLE IIIA. Internal vibrational modes of the OH^- groups.

Molecular sym.		Site sym.		Factor group sym.	
$C_{\infty v}$	$N = 2$ →	C_s	→	C_{2h}	
t^v	f^v				a^v
1	Σ^+ — 2 —	A'		A_g	1
				B_u	1

and $M(3)$ site occupancy of the Fe^{2+} for the quaternary system is given by:

$$\begin{aligned} Fe^{2+}(M(1), M(3)) &= 2\phi_1 + \phi_3 \\ &= (B + 2C + 3D + F + 2H + I \\ &\quad + 2M + O + L + Q)/W. \end{aligned} \quad (11)$$

However, the occupancy for each site can be approximated by assuming that $B'' = C''$, $E'' = G''$, . . . , etc. As an example, the occupancy of the $M(1)$ site and that of the $M(3)$ site for the binary system are given, respectively, by:

$$\mu_1 = \frac{2(A + B)}{A + B + C + D} \qquad \mu_3 = \frac{A + C}{A + B + C + D} \quad (12a)$$

$$\phi_1 = \frac{2(C + D)}{A + B + C + D} \text{ and } \phi_3 = \frac{B + D}{A + B + C + D} \quad (12b)$$

where μ_i is the occupancy of Mg^{2+} on the $M(i)$ site, ϕ_i is the occupancy of Fe^{2+} on the $M(i)$ site (also ψ_i for Fe^{3+}, α_i for Al^{3+}), and A, B, C, and D are the relative integrated intensities of the bands corresponding to the A, B, C, and D configurations.

In the above discussion the preference of certain cations to occupy a given site has not been considered. If it exists, the situation becomes more complicated, as was discussed previously.[9,15] For a binary system, the simplest case, this preference can be described by introducing the segregation parameters defined by:

$$S_f = \phi_1 - \phi_3 \quad (13a)$$

$$S_m = \mu_1 - \mu_3. \quad (13b)$$

The conditions $\phi_1 + \mu_1 = 1$ and $\phi_3 + \mu_3 = 1$ yield the relation $S_f = -S_m$. The following set of equations represents another expression for the site occupancy which is equivalent to the last row of Table V, where I_A, I_B, I_C, and I_D are the normalized integrated intensities of the corresponding bands:

$$I_A = \mu_1^2\mu_3 = (1 - S_f - \phi_3)^2(1 - \phi_3) \quad (14a)$$

$$\begin{aligned} I_B &= \mu_1^2\phi_3 + 2\mu_1\phi_1\mu_3 \\ &= (1 - S_f - \phi_3)^2\phi_3 + 2(1 - S_f - \phi_3) \\ &\quad \cdot(S_f + \phi_3)(1 - \phi_3) \end{aligned} \quad (14b)$$

$$\begin{aligned} I_C &= \phi_1^2\mu_3 + 2\mu_1\phi_1\mu_3 \\ &= (S_f + \phi_3)^2(1 - \phi_3) + 2(1 - S_f - \phi_3) \\ &\quad \cdot(S_f + \phi_3)\phi_3 \end{aligned} \quad (14c)$$

and

$$I_D = \phi_1^2\phi_3 = (S_f + \phi_3)^2\phi_3. \quad (14d)$$

Figure 4 is the graphical expression for this set of equations, in which the total occupancy of the Fe^{2+} cation in the $M(1)$ and $M(3)$ sites is represented by T_f, an additional parameter. The preferential distribution of cations between the $M(1)$ and $M(3)$ sites can be estimated graphically for the binary system. An attempt has been made to establish similar expressions for ternary and quaternary systems, but the number of variables involved requires multidimensional space to represent the results.

EXPERIMENTS AND RESULTS

The five samples which were studied in this work belong to four principal amphibole groups. Their chemical formulas have been determined by elemental analysis (both wet-chemical and electron-microprobe analysis), as shown in Table VI.

The Raman microspectroscopic measurements were performed on the MOLE (Jobin-Yvon, France). Because all the samples consisted of very small crystals ($d \sim 30$ μm), and some of them had rather high fluorescence levels, a point-illumination mode was used to choose the excited area near the surface of the sample which had the lowest fluorescence. The resulting improved signal-to-noise ratio yielded spectra which were especially valuable for the analysis of the OH bands of the amphiboles. The 5145 Å line of an argon-ion laser was used for excitation, and the spectral resolution of the instrument was 2 cm^{-1}.

Under these conditions the Raman spectra of five amphibole samples were obtained. In the low-frequency region (1200–100 cm^{-1}) the spectra corresponding to the

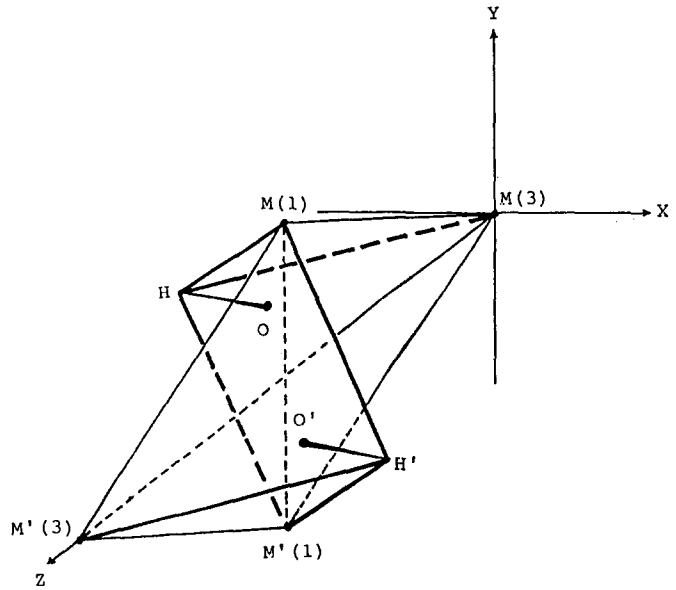

FIG. 3. Local environment of the two OH^- ions in the Cummingtonite lattice.

TABLE V. Occupational situation of $M(1)$, $M(3)$ sites.

System	OH^- stretching band		Configuration	Occupancy of site by cations									
							Mg^{2+} ○		Fe^{2+} ⊕		Fe^{3+} ◎		Al^{3+} ●	
				$M(1)$		$M(3)$	$M(1)$	$M(3)$	$M(1)$	$M(3)$	$M(1)$	$M(3)$	$M(1)$	$M(3)$
Binary	A		$3\,Mg^{2+}$	○	○	○	2	1						
	B	B'	$2\,Mg^{2+}Fe^{2+}$	○	○	⊕	2			1				
		$2B''$		⊕	○	○	2	2	2					
	C	C'	$Mg^{2+}2\,Fe^{2+}$	⊕	⊕	○		1	2					
		$2C''$		○	⊕	⊕	2		2	2				
	D		$3\,Fe^{2+}$	⊕	⊕	⊕			2	1				
Ternary	E	E'	$2\,Mg^{2+}Fe^{3+}$	○	○	◎	2					1		
		$2E''$		◎	○	○	2	2			2			
	G	G'	$Mg^{2+}2\,Fe^{3+}$	◎	◎	○		1			2			
		$2G''$		○	◎	◎	2				2	2		
	F	$2F''_1$	$Mg^{2+}Fe^{2+}Fe^{3+}$	○	⊕	◎	2		2			2		
		$2F''_2$		⊕	◎	○		2	2		2			
		$2F''_3$		○	◎	⊕	2			2	2			
	H	H'	$2\,Fe^{2+}Fe^{3+}$	⊕	⊕	◎			2			1		
		$2H''$		◎	⊕	⊕			2	2	2			
	I	I'	$Fe^{2+}2\,Fe^{3+}$	◎	◎	⊕				1	2			
		$2I''$		⊕	◎	◎			2		2	2		
	J		$3\,Fe^{3+}$	◎	◎	◎					2	1		
Quaternary	K	K'	$2\,Mg^{2+}Al^{3+}$	○	○	●	2							1
		$2K''$		●	○	○	2	2					2	
	N	N'	$Mg^{2+}2\,Al^{3+}$	●	●	○		1					2	
		$2N''$		○	●	●	2						2	2
	M	M'	$2\,Fe^{2+}Al^{3+}$	⊕	⊕	●			2					1
		$2M''$		●	⊕	⊕			2	2			2	
	O	O'	$Fe^{2+}2\,Al^{3+}$	●	●	⊕				1			2	
		$2O''$		⊕	●	●			2				2	2
	S	S'	$2\,Fe^{3+}Al^{3+}$	◎	◎	●					2			1
		$2S''$		●	◎	◎					2	2	2	
	R	R'	$Fe^{3+}2\,Al^{3+}$	●	●	◎						1	2	
		$2R''$		◎	●	●					2		2	2
	P	$2P''_1$	$Mg^{2+}Al^{3+}Fe^{3+}$	○	◎	●	2				2			2
		$2P''_2$		◎	●	○		2			2		2	
		$2P''_3$		○	●	◎	2					2	2	
	L	$2L''_1$	$Mg^{2+}Al^{3+}Fe^{2+}$	○	⊕	●	2		2					2
		$2L''_2$		⊕	●	○		2	2				2	
		$2L''_3$		●	○	⊕	2			2			2	
	Q	$2Q''_1$	$Fe^{2+}Al^{3+}Fe^{3+}$	⊕	◎	●			2		2			2
		$2Q''_2$		◎	●	⊕				2	2		2	
		$2Q''_3$		●	⊕	◎			2			2	2	
	T		$3\,Al^{3+}$	●	●	●							2	1

$Z(XX)\bar{Z}$ and $Z(XY)\bar{Z}$ configurations were measured with the use of a polarization rotator (half-wave plate) and an analyzer. Because of the small size of the samples, they could not be oriented. However, by choosing the direction X of the electric vector for which the highest intensity was obtained for the symmetric Raman band $\nu_1(A_g)$ at 670 cm^{-1}, it was possible to establish the corresponding relationship between the crystallographic axis of the sample and the laboratory coordinates. It is clear that in each spectrum there are two groups of bands whose intensity changes in different ways when the direction of the electric vector is changed from X to Y. Application of the Raman polarizability tensor of the C_{2h} point group (crystal class)

$$\begin{pmatrix} a & & d \\ & b & \\ d & & c \end{pmatrix}$$

for the A_g species and

$$\begin{pmatrix} & e & \\ e & & f \\ & f & \end{pmatrix}$$

for the B_u species allows the symmetries of the modes corresponding to the principal bands to be distinguished (see Fig. 5). However, it is still difficult to assign all the bands and even to find enough bands in the spectra to account for the 60 predicted Raman-active modes.

In the spectral region 3500–3800 cm^{-1}, all the bands which correspond to the stretching of the OH groups of the amphiboles have been recorded (Fig. 6). In order that the signal-to-noise ratio in these spectra could be improved, the averaging of six to nine spectra was systematically made. As indicated above, all these Raman-active modes have A_g symmetry. Therefore, when the incident polarization is modified, their intensities should change in the same way, as was verified in the experiments. Thus the relative intensities can serve as the basis for the determination of site occupancy.

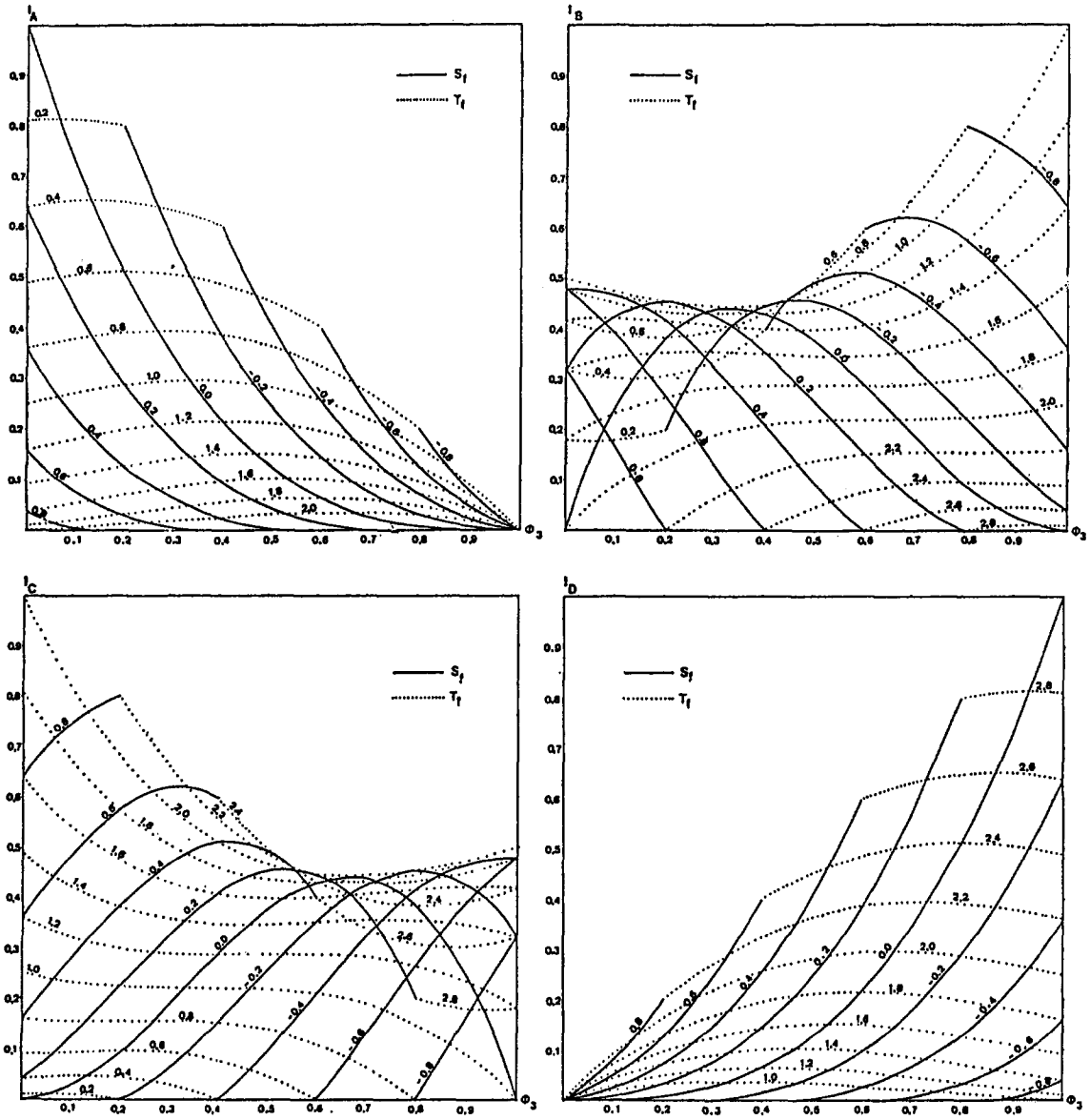

FIG. 4. Calculated correlations between the Raman intensities I_A, I_B, I_C, and I_D, and the occupancy ϕ_3 of Fe^{2+} on the $M(3)$ site, where S_f is the segregation parameter.

After digitalization, the five OH spectral regions were analyzed on a MINI-6 computer with the use of a decomposition program. The program can adjust the profile of the spectral region by changing the proportions of Gaussian and Lorentzian components in the calculated curve. The final results of the calculation are shown in Fig. 7. The assignments were made by reference to the work of Hawthorne.[14] From Table VII, it can be seen that the assignments are reasonable. For the magnesio-hornblende sample, the treatment of the spectrum was very

TABLE VI. Chemical compositions of the amphibole samples.

Amphibole sample	Classification	Chemical formula
Cummingtonite	Iron-magnesium-manganese amphibole	$(K_{0.0039}Na_{0.0148}Ca_{0.1507}Mn_{0.0622}Mg_{3.4478}Fe_{3.2852}Al_{0.0166}Cr_{0.0060}Ti_{0.0011})$ $(Al_{0.0122}Si_{7.9878})$ O_{22} $((OH)_{1.9855}F_{0.0145})$
Actinolite	Calcic amphibole	$(Na_{0.051}Ca_{1.531}Mn_{0.094}Mg_{3.647}Fe_{1.343}Al_{0.127})$ $(Al_{0.060}Si_{7.940})$ O_{22} $((OH)_{1.989}O_{0.011})$
Winchite	Sadic-calcic amphibole	$K_{0.104}$ $(Na_{0.831}Ca_{1.247}Mg_{3.265}Fe_{1.438}Al_{0.124})$ $(Al_{0.046}Si_{7.954})$ O_{22} $((OH)_{1.784}O_{0.216})$
Glaucophane	Alkali amphibole	$(K_{0.0127}Na_{0.0141})$ $(Na_{1.7910}Ca_{0.1526}Mn_{0.0014}Mg_{2.0984}Fe_{1.0889}Al_{1.8652}Cr_{0.0013}$- $Ti_{0.0012})$ $(Al_{0.3040}Si_{7.6960})$ O_{22} $((OH)_{1.9905}F_{0.0995})$
Magnesio-hornblende	Calcic amphibole	$(K_{0.1477}Na_{0.1555})$ $(Na_{0.0831}Ca_{1.8875}Mn_{0.0356}Mg_{2.8198}Fe_{1.6928}Al_{0.3689}Ti_{0.1016}$- $Cr_{0.0107})$ $(Al_{0.9734}Si_{7.0266})$ O_{22} $((OH)_{1.9146}F_{0.0854})$

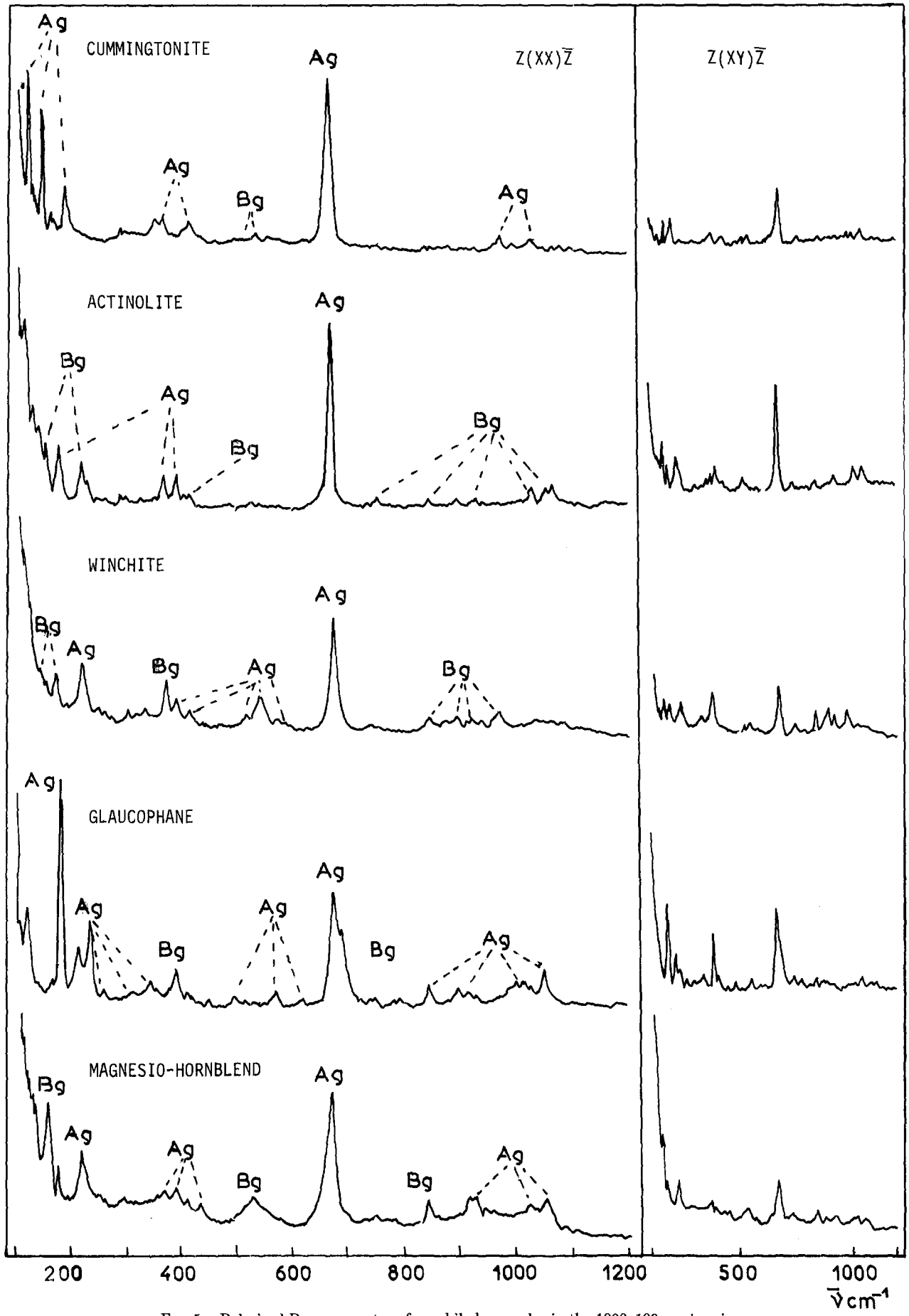

FIG. 5. Polarized Raman spectra of amphibole samples in the 1200–100 cm^{-1} region.

difficult because of the presence of a broad band. After the sample was heated at 120°C for 24 h, the broad band was still observed. Although the assignment of this feature to water absorption cannot be excluded, the broad band may well arise from the presence of other cations in the $M(1)$ and $M(3)$ sites. As indicated above, the entrance of four types of cation leads to 20 different configurations in the $M(1)$ and $M(3)$ sites. If there are five or six types of cation, the number of configurations will increase rapidly and the resulting bands will overlap to yield a large spectral feature. Thus, for these types of amphibole the application of spectroscopic methods has certain limitations.

From the results of the spectral fitting calculations, the total occupancy of the $M(1)$ and $M(3)$ sites can be found for each cation, while the occupancy of each site can only be approximately determined, as shown in Table VIII. These results indicate that the approximation which was used for determining μ_i, ϕ_i, ..., etc., has no influence on the estimation of total occupancy, but small changes in the distributions of each cation in the $M(1)$ and $M(3)$ sites may occur, as shown below.

Cummingtonite is the simplest sample in the series considered here. By neglecting the small amount of Fe^{3+} in the $M(3)$ site, one can consider it to be a purely binary system. If it is assumed that the Fe^{2+} and Mg^{2+} ions are distributed randomly between the $M(1)$ and $M(3)$ sites, the following form of the site occupancy formula described earlier can be obtained:

$$T_f = 2\phi_1 + \phi_3 = 1.427, \qquad \phi_3 = 0.497. \qquad (15)$$

However, if Fig. 4 is used to determine the value of ϕ_3 graphically in order to place measured values of I_A, I_B, I_C, and I_D on the curves corresponding to $S_f = 0$ (random distribution), then the value of ϕ_3 which is obtained lies between 0.490 (A, C) and 0.465 (B, D). These results show that the approximations in deducing the cation occupancy for each site introduce some errors into the results.

On the other hand, if preferential cation occupancy of the different sites is considered, then with the use of the normalized values of I_A, I_B, I_C, and I_D, and the calculated value of T_f, which is not subject to any approximation, the graphical analysis yields two values of S_f and, therefore, two sets of site occupancy values: μ_1, μ_3, and ϕ_1, ϕ_3. As both solutions seem reasonable, a choice cannot be made.

It is concluded that within the limitations of the experimental data obtained in this work, or with the use of the infrared data given in the literature, the exact values of μ_i and ϕ_i are impossible to obtain. The only solution to this problem is in future experiments to attempt the resolution of the B', B'' and C', C'' spectral components.

CONCLUSIONS

This work describes the first attempt to determine cation distributions in amphiboles by Raman microspectroscopy. The Raman spectra which were obtained for the OH stretching region have higher resolution than the infrared spectra reported previously. However, even with the use of the most sophisticated Raman instruments, it

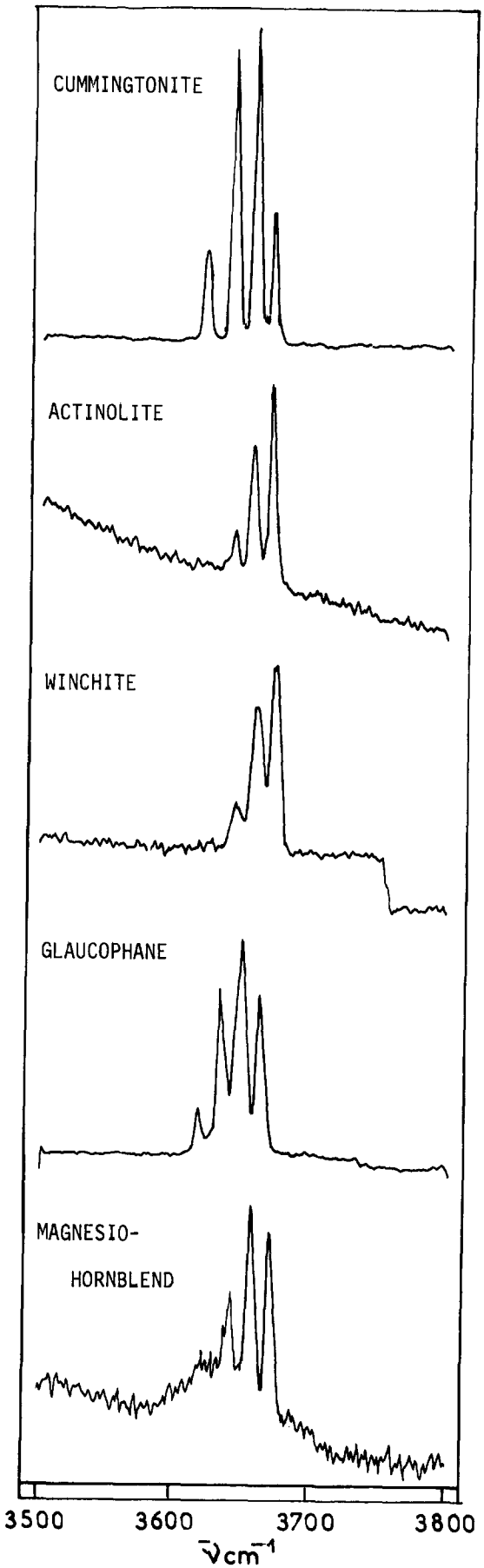

FIG. 6. Raman spectra of amphibole samples in the 3500–3800 cm^{-1} region.

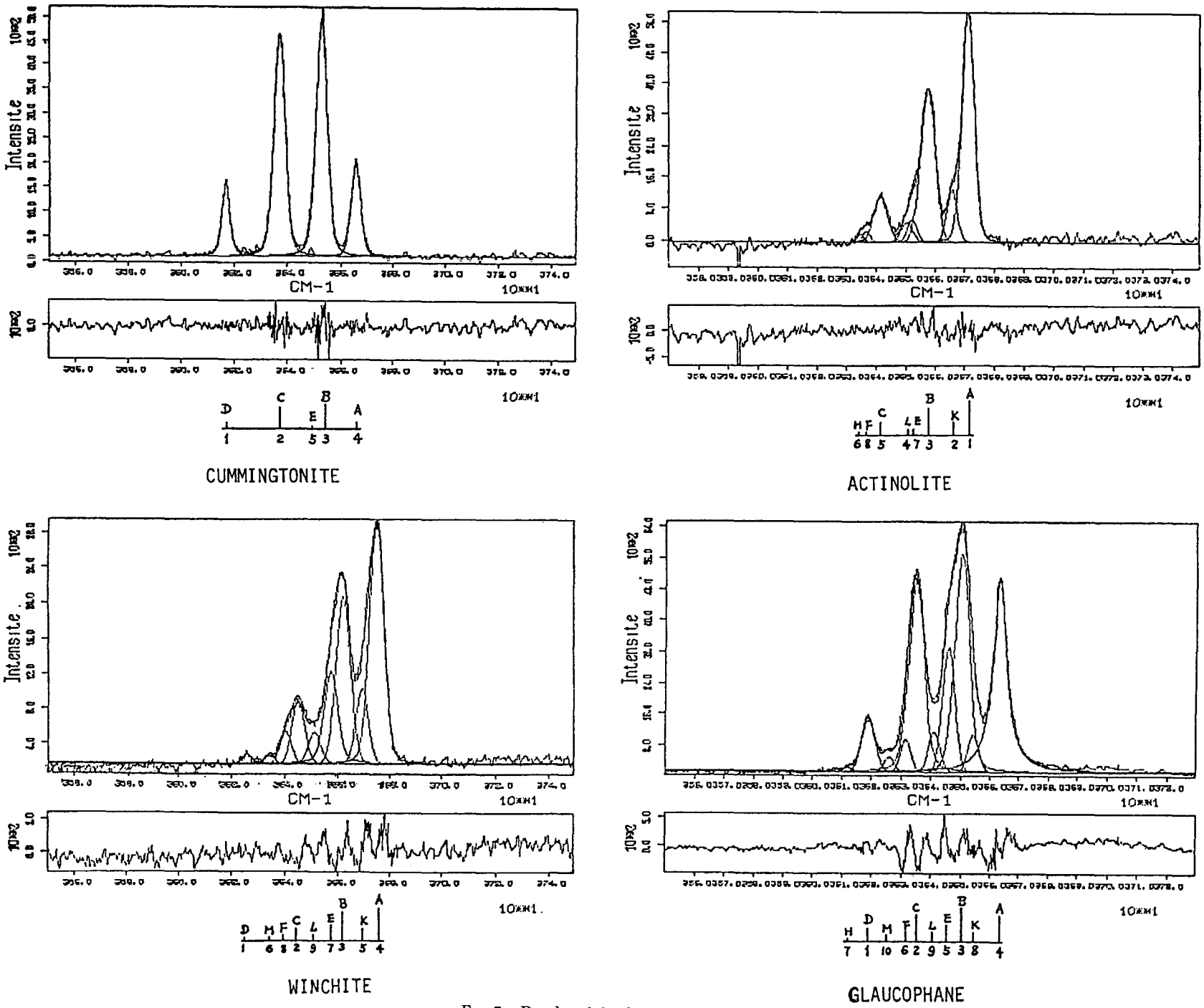

FIG. 7. Results of the decomposition calculation.

TABLE VII. Band positions and assignments.

	Configuration	Cummingtonite		Actinolite		Winchite		Glaucophane	
		Position		Position		Position		Position	
A	$3\,Mg^{2+}$	3665.87	0	3671.10	0	3674.60	0	3663.30	0
B	$2\,Mg^{2+}Fe^{2+}$	3652.90	−13.0	3657.50	−13.6	3661.80	−12.8	3650.40	−12.9
C	$Mg^{2+}2\,Fe^{2+}$	3637.06	−28.8	3641.66	−29.4	3644.90	−29.7	3535.10	−28.2
D	$3\,Fe^{2+}$	3616.75	−49.1			3625.50	−49.1	3619.00	−44.3
E	$2\,Mg^{2+}Fe^{3+}$	3648.88	−17.0	3652.30	−18.8	3657.20	−17.4	3646.00	−17.3
F	$Mg^{2+}Fe^{2+}Fe^{3+}$			3636.80	−34.3	3640.10	−34.5	3631.60	−31.7
H	$2\,Fe^{2+}Fe^{3+}$							3612.10	−51.2
K	$2\,Mg^{2+}Al^{3+}$			3665.70	−5.4	3669.00	−5.6	3654.30	−9.0
L	$Mg^{2+}Fe^{2+}Al^{3+}$			3650.50	−20.6	3651.00	−23.6	3641.20	−22.1
M	$2\,Fe^{2+}Al^{3+}$			3634.80	−36.3	3633.90	−40.7	3626.00	−37.3

was not possible to distinguish the bands due to the different cation arrangements of one particular configuration. It is apparent that the widths of the expected bands are greater than the spectral resolution of the instrument used and that their overlap precludes the possibility of resolving them under the conditions of the experiment. Nevertheless, the experimental results and the theoretical analysis developed in this work provide a better understanding of the problems involved in the determination of the cation distributions in amphiboles with the use of vibrational spectroscopic methods.

In future work, low-temperature experiments will be carried out in an attempt to separate the B', B'' and C', C'' band components. Calculations are now being made of the changes in the local force field of the OH groups due to the different cation distributions in the $M(1)$ and $M(3)$ sites. The latter work should lead to a more detailed interpretation of the observed band pattern in the OH stretching region.

TABLE VIII. Results of the site occupancy calculation.

		Cummingtonite	Actinolite	Winchite	Glaucophane
Mg^{2+}	Total	1.5752	2.2732	2.1839	1.8600
	$2\mu_1$	1.0746	1.7426	1.7177	1.3403
	μ_3	0.5006	0.5306	0.4661	0.5197
Fe^{2+}	Total	1.4199	0.5594	0.5050	0.9361
	$2\varphi_1$	0.9254	0.2279	0.2337	0.6229
	φ_3	0.4945	0.3315	0.2714	0.3132
Fe^{3+}	Total	0.0049	0.0498	0.1749	0.1328
	$2\psi_1$		0.0074	0.0239	0.0153
	ψ_3	0.0049	0.0424	0.1510	0.1175
Al^{3+}	Total		0.1176	0.1326	0.0711
	$2\xi_1$		0.0222	0.0247	0.0215
	ξ_3		0.0955	0.1115	0.0496

ACKNOWLEDGMENTS

This work was carried out in the Laboratory of Infrared and Raman Spectrochemistry [LASIR-CNRS (LP. 2641)], France, under a scientific cooperation program between CNRS and the Chinese Ministry of Geological Deposits. The authors would like to express their appreciation to Guo Lihe of the Chinese Academy of Geological Sciences for many helpful suggestions and the donation of the amphibole samples. B. De Bettignies is especially thanked for his development of the band decomposition program. Mrs. Wang would like to express her thanks to her colleagues at LASIR for their collaboration and kindness during her visit.

1. G. M. Bancroft and A. G. Maddock, Amer. Mineral. **52,** 1009 (1967).
2. G. M. Bancroft, *Mössbauer Spectroscopy: An Introduction for Inorganic Chemists and Geochemists* (McGraw-Hill, New York, 1973).
3. A. D. Law, Bull. Mineral. **104,** 381, 423 (1981).
4. R. G. Burns and R. G. J. Strens, Science **153,** 890 (1966).
5. R. G. Burns and F. J. Prentice, Amer. Mineral. **53,** 770 (1968).
6. R. G. Burns and C. J. Greaves, Amer. Mineral. **56,** 2010 (1971).
7. R. G. J. Strens, "The Common Chain, Ribbon and Ring Silicates," in *The Infrared Spectra of Minerals,* V. C. Farmer, Ed. (Mineralogical Society, London, 1974), pp. 305–330.
8. R. G. J. Strens, Chem. Comm. **15,** 519 (1966).
9. A. D. Law, "A Model for the Investigation of Hydroxyl Spectra of Amphiboles," in *The Physics and Chemistry of Minerals and Rocks,* R. G. J. Strens, Ed. (Wiley, London, 1976), pp. 677–686.
10. W. B. White, "Structural Interpretation of Lunar and Terrestrial Minerals by Raman Spectroscopy," in *Infrared and Raman Spectroscopy of Lunar and Terrestrial Minerals,* Clarence Karr, Jr., Ed. (Academic Press, New York, 1975), Chap. 13, pp. 325–356.
11. J. J. Blaha and G. J. Rosasco, Anal. Chem. **50,** 892 (1978).
12. B. W. Cook and G. D. Ogilvie, "Micronanalysis of Industrial Polymers by Raman Spectroscopy," in *Microbeam Analysis,* K. F. J. Heinrich, Ed. (San Francisco Press, San Francisco, 1982), pp. 294–300.
13. S. Ghose, Acta Cryst. **14,** 622 (1961).
14. F. C. Hawthorne, "Amphibole Spectroscopy," in *Reviews in Mineralogy, 9A,* D. Veblen, Ed. (Mineralogical Society of America, Washington, D.C., 1981), pp. 103–139.
15. E. J. W. Whittaker, Phys. Chem. Minerals **4,** 1 (1979).